ACS MEASUREMENT SCIENCE Au
AN OPEN ACCESS JOURNAL OF THE AMERICAN CHEMICAL SOCIETY

pubs.acs.org/measureau
Article

Automated Analysis of Extracellular Matrix Invasion of Cancer Cells from Tumor Spheroids

Jacob Heiss and Hossein Tavana*

Cite This: ACS Meas. Sci. Au 2024, 4, 260−266
Read Online

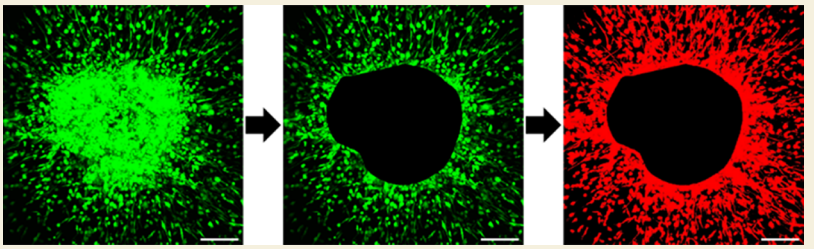

ABSTRACT: The main cause of mortality among cancer patients is metastatic disease. Metastasis develops from cancer cells that invade the stromal tissue and intravasate the circulatory or lymphatic systems to eventually form new tumors in other organs. Blocking cancer cell invasion can potentially prevent or reduce the metastatic progression of cancers. Testing different chemical compounds against cell invasion in three-dimensional cultures is a common laboratory technique. The efficacy of the treatments is often evaluated from confocal microscopic images of the cells using image processing. However, the analysis approaches are often subject to variations and inconsistencies due to user decisions that must be made while processing each image. To overcome this limitation, we developed a fully automated method to quantify the invasion of cancer cells from a 3D tumor spheroid into the surrounding extracellular matrix. We demonstrated that this method resolves cell invasion from spheroids of different shapes and sizes and from cells that invade as a cluster or individually. We also showed that this approach can help quantify the dose-dependent anti-invasive effects of a commonly used chemotherapy drug. Our automated method significantly reduces the time and increases the consistency and accuracy of cancer cell invasion analysis in three-dimensional cultures.

KEYWORDS: *breast cancer, image analysis, cancer invasion, automation, tumor model*

INTRODUCTION

Metastasis is the leading cause of death among cancer patients and accounts for over 90% of all mortalities.[1] Cancer cells disseminated away from the primary tumor may form local metastases or eventually grow into new tumors in other organs. A key process to facilitate metastasis is the local migration and invasion of cancer cells into the surrounding tissue to access the blood or lymphatic vessels. Invading cancer cells often undergo full or partial epithelial-to-mesenchymal transition (EMT) and acquire a spindle-shaped mesenchymal morphology for effective motility.[2] EMT of cancer cells may result from several factors including autocrine TGF-β and Wnt signaling, paracrine HGF and TGF-β signaling with stromal cells such as cancer-associated fibroblasts, downregulation of epithelial junctional proteins such as E-cadherin, and upregulation of mesenchymal markers including N-cadherin, vimentin, or fibronectin.[3] Invasive breast cancer cells may also gain a stem cell-like state and show resistance to cytotoxic chemotherapies and targeted therapies.[4−6]

To migrate and invade through 3D environments, cancer cells move through dense and complex extracellular matrix (ECM) structures and undergo specific adaptations. Besides navigating through diverse ECM environments and overcoming extracellular barriers, cancer cells invade the surrounding stromal tissue using various mechanisms. Invasion may occur by single cells that assume a mesenchymal or amoeboid morphology. Cancer cells with a mesenchymal morphology proteolytically degrade the surrounding ECM and generate paths for invasion, whereas cells with an ameboid morphology squeeze through confined spaces in the ECM without the need to remodel it. Cancer cells also have the plasticity to transition between these two states.[7] In addition to single cell invasion, cancer cells may invade the surrounding ECM collectively as a sheet or a strand/cluster where cells maintain their mechanical coupling via cell−cell adhesions.[8]

Due to the critical role of cell invasion in cancer metastasis, therapeutic targeting of this process is expected to improve outcomes for patients.[9] Understanding different molecular

Received: October 30, 2023
Revised: December 8, 2023
Accepted: December 8, 2023
Published: December 28, 2023

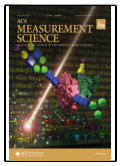

https://doi.org/10.1021/acsmeasuresciau.3c00064
ACS Meas. Sci. Au 2024, 4, 260−266

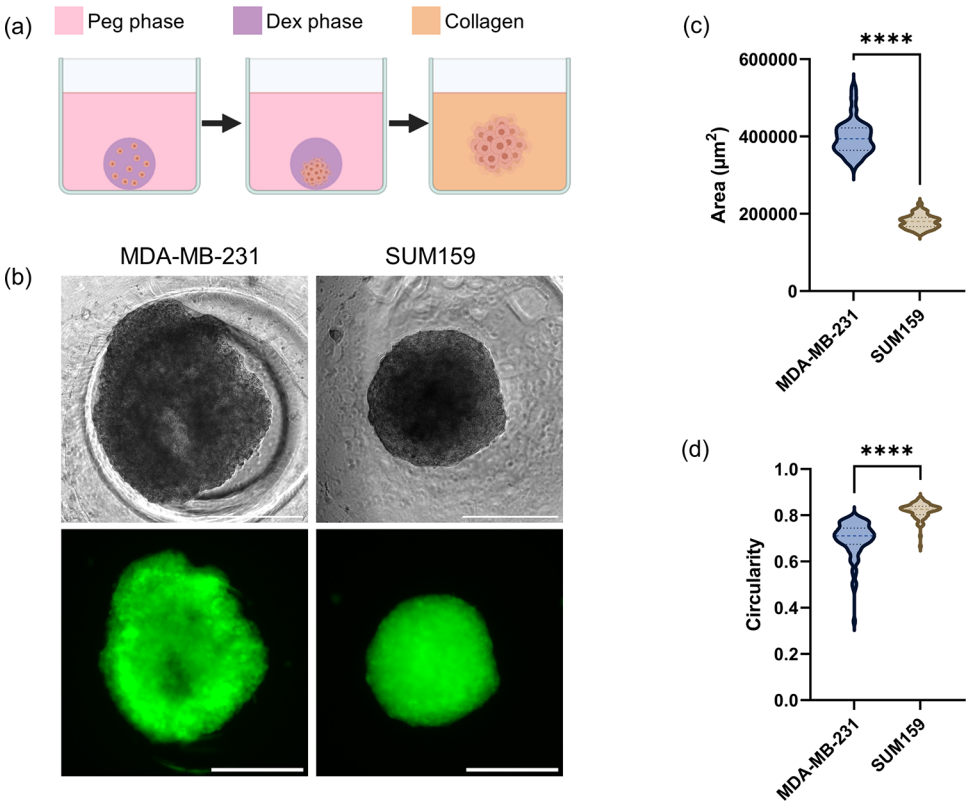

Figure 1. (a) Schematics of aqueous two-phase system technology to form collagen-embedded tumor spheroid cultures. (b) Phase and GFP fluorescent microscope images of MDA-MB-231 and SUM159 TNBC spheroids. (c) Projected areas and (d) circularities of MDA-MB-231 and SUM159 spheroids. Scale bars are 200 μm.

mechanisms that facilitate cancer cell invasion is critical to develop preventive strategies against metastatic disease progression. Cell-based assays are often used to study the effects of various treatments against migration and invasion of cancer cells and identify the underlying inhibitory mechanisms of effective compounds. The most basic assay uses a monolayer (2D) culture of cancer cells containing a circular or scratched acellular area into which cells migrate, mimicking wound healing.[10,11] The use of a transwell system also allows the migration of cancer cells through a porous membrane toward a chemotactic agent in the bottom well. However, these 2D assays do not represent cell invasion in 3D environments. To achieve physiological relevance, more complex models have been developed, mainly using microfluidic devices or hydrogels. While microfluidic models allow for greater complexities such as compartmentalized tumor and vasculature to study processes such as intravasation or extravasation,[12] hydrogel-based models often made in conventional microwell plates are compatible with automated liquid handling to allow for high throughput drug testing applications.[13]

Once an invasion assay is completed and the images of cells are collected, in most cases, the user may apply manual or semiautomated methods to the images to quantify cell invasion. The primary methods of quantifying 3D cell invasion involve measuring the distance of cell migration from a reference point, counting the number of invading cells, mapping the directions of cell invasion, and determining the invading area of cells.[14−16] One of the main hurdles with all these manual and semi-automated methods is that they are highly time-consuming to perform and create a bottleneck for high throughput experiments of drug testing against cell invasion, while automated methods are often extremely specific in the context that they measure invasion.[17] In addition, because in many methods, all or part of the analysis is often performed by hand, there is significant room for human errors. Differences in analysis methods among researchers can also skew the results.

To address the low speed and inconsistency associated with existing methods, we developed an algorithm to automate the process of quantifying cancer cell invasion in a 3D hydrogel ECM environment from confocal microscopy images. We validated this new method by demonstrating its utility across breast cancer cells with different invasion modalities and for drug screening applications against cancer cell invasion.

MATERIALS AND METHODS

Cell Culture

MDA-MB-231 and SUM159 triple negative breast cancer (TNBC) cell lines transfected to stably express a green fluorescent protein (GFP) were kindly provided by Dr. Gary D. Luker (University of Michigan). MDA-MB-231 cells were cultured in Dulbecco's modified Eagle's medium (DMEM) (Sigma). SUM159 cells were cultured in Ham's F-12 medium (Gibco). Media were supplemented with 10% fetal bovine serum (Sigma), 1% glutamax (Sigma), and 1% antibiotic/antimycotic (Life Technologies). The cells were plated in culture flasks and kept in an incubator at 37 °C with 5% CO_2. When the cells proliferated to a 80−90% confluence monolayer, they were rinsed with phosphate-buffered saline (Sigma) and detached from the flask using 0.25% trypsin (Life Technologies). The cell suspension was collected in a 15 mL centrifuge tube and centrifuged down for 5 min at 174 rcf. After aspirating the supernatant, the cell pellet was resuspended in the respective complete culture medium. The cell suspension was used to continue the culture.

https://doi.org/10.1021/acsmeasuresciau.3c00064
ACS Meas. Sci. Au 2024, 4, 260−266

Spheroid Formation

Spheroids of cancer cells were made using an aqueous two-phase system (Figure 1a).[18] The ATPS consisted of 5%(w/v) of 35 kDa polyethylene glycol (PEG) and 6.4% (w/v) of 500 kDa dextran with culture media used as the solvent.[19] Cells were first suspended in 12.8% (w/v) dextran solution at 50% of the final desired volume. Then, 49% of the final volume of media was added with 1% of 3.1 mg/mL human type I collagen (Advanced Biomatrix). This resulted in a final density of 1.0×10^4 cells/0.3 μL. Using an Agilent Bravo 2 robotic liquid handler, 30 μL of the 5% (w/v) PEG phase solution was added to the wells of a round-bottom 384-well plate (Corning). Then, 0.3 μL of the cell suspension in DEX phase solution was robotically aspirated and dispensed into each well to form a DEX phase drop containing the cells. The DEX phase drop settled to the bottom of the well and remained phase separated from the immersion PEG phase. Cells remained confined to the DEX phase drops and formed spheroids within 2−4 days of incubation.

Area and Circularity of Spheroids

Spheroids were imaged using an inverted fluorescence microscope (Axio Observer A1, Zeiss) in the round-bottom 384-well plates. The surface area of each spheroid was calculated from its fluorescent image in FIJI (ImageJ). The circularity of each spheroid was calculated by measuring the perimeter of each spheroid in FIJI and using $circularity = 4\pi \times area/perimeter^2$.

Spheroid Encapsulation in Collagen

Spheroids were encapsulated in a collagen matrix. Human type I collagen at 6 (mg/mL) (Lifecore Biomedical) was diluted down to 5.22 (mg/mL) and balanced to a pH of 7, following the manufacturer's protocols. The diluted collagen was loaded into a flat-bottom 96-well plate (Thermo Fisher), which was kept on a cooling plate inside a cell culture hood to prevent premature collagen gelation. The liquid handler was programmed to aspirate each spheroid with 7 μL of medium and then aspirate 23 μL of the collagen solution, bringing the final concentration of collagen to 4 mg/mL. The liquid handler dispensed the collagen solution and spheroid into a glass-bottom 384-well plate (MatTek Life Sciences). The cultures were incubated for 90 min to allow the collagen to gel and then supplemented with 30 μL of complete growth media.

Drug Treatments

Paclitaxel was purchased from Selleckchem, dissolved in dimethyl sulfoxide, aliquoted, and stored at −20 °C. The collagen-encapsulated spheroids were treated with paclitaxel immediately after collagen gelation at the following concentrations: 0 nM (negative control), 10^{-2}, 10^{-1}, 10^0, 10^1, 10^2, 10^3, 10^4, and 10^5 nM. Cancer cells were allowed to invade from spheroids into the collagen matrix for 4 days for MDA-MB-231 cells and for 6 days for SUM159 cells. In each case, the medium was refreshed every other day. A nonlinear regression was used to construct a dose−response curve for each cell line.

Confocal Microscopy

Invasion of cells in the 3D collagen matrix was imaged at 10× magnification using a Nikon A1 confocal microscope. A 488 nm laser with a 500 nm-550 nm filter was used to capture the GFP^+ cancer cells. A slice thickness of 20 μm was used with 10−40 slices per spheroid depending on the spheroid size. The images were loaded into FIJI for post-processing.

Statistics

Statistical analysis was performed by using GraphPad Prism. R^2 values were calculated based on a linear regression. A one-way ANOVA with a posthoc Tukey's test was used when comparing multiple groups. Dose−response curves were generated using a nonlinear regression (curve fit) with a variable slope. The dose−response curves were also used to calculate the 50% inhibitory concentration (IC50) of the drug and the area under the curve (AUC) with each cell line. All error bars represent the standard deviation for each sample. Statistical significance was defined at $p < 0.05$.

RESULTS AND DISCUSSION

Quantifying the Morphology and Size of Breast Cancer Spheroids

We measured and compared the morphology of MDA-MB-231 and SUM159 spheroids with a 1.0×10^4 cell density from both phase and GFP fluorescence images (Figure 1b). MDA-MB-231 spheroids had a mean area of 3.98×10^5 μm^2 and a circularity of 0.70 ± 0.08, whereas SUM159 spheroids had a mean area of 1.80×10^5 μm^2 and a circularity of 0.82 ± 0.03 (Figure 1c,d). These data indicate that SUM159 cells formed significantly more compact and round spheroids than MDA-MB-231 cells did ($p < 0.0001$). We have previously shown that spheroids formed with the aqueous two-phase system technology are about 30% more round and compact compared to those from standard ultralow attachment plates.[20] This is because cells remain within a round nanodrop of the aqueous DEX phase, which is immersed in a bath of the aqueous PEG phase, for several days. Producing more round spheroids reduces spatial heterogeneity of available oxygen and hypoxia within the spheroid, and thus reduces additional effects on cell invasion.[21] This is especially important for cell lines, such as MDA-MB-231 that do not tend to aggregate well. We note that there are other software programs that can provide measurements besides size and circularity.[22,23]

Invasion of Breast Cancer Cells in a 3D ECM

MDA-MB-231 and SUM159 TNBC cells showed strikingly different patterns of invasion in the collagen matrix. MDA-MB-231 cells mainly invaded the ECM as single cells. Invading cells dispersed relatively uniformly in collagen and showed both elongated and round morphologies. In contrast, SUM159 cells mainly invaded in clusters and protruded out of spheroids with spikelike morphologies, although there were also a small number of individually invading cells with both elongated and round morphologies (Figure 2). These cell lines are Claudin-low and Basal B-type breast cancer cells that identify as TNBC.[24,25] Cells from both lines have a mesenchymal-like appearance, consistent with the elongated morphology of the majority of cells in the invading front. The small number of invading cells with a round morphology may represent an amoeboid-like motility through confined spaces within the ECM.[7] Unlike mesenchymal cell

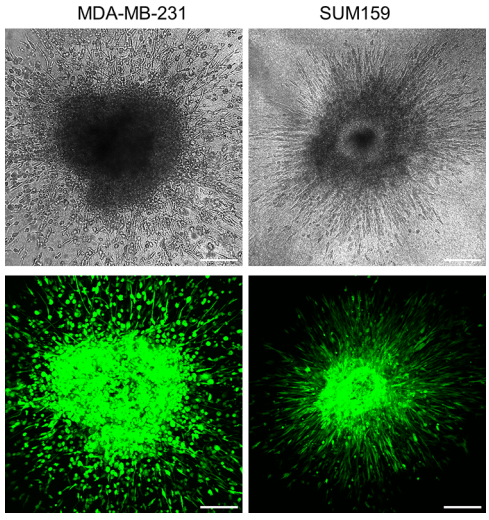

Figure 2. Phase and fluorescent confocal microscope images of the collagen invasion of cells from MDA-MB-231 (day 4) and SUM159 (day 6) spheroids. Scale bars are 200 μm.

https://doi.org/10.1021/acsmeasuresciau.3c00064
ACS Meas. Sci. Au 2024, 4, 260−266

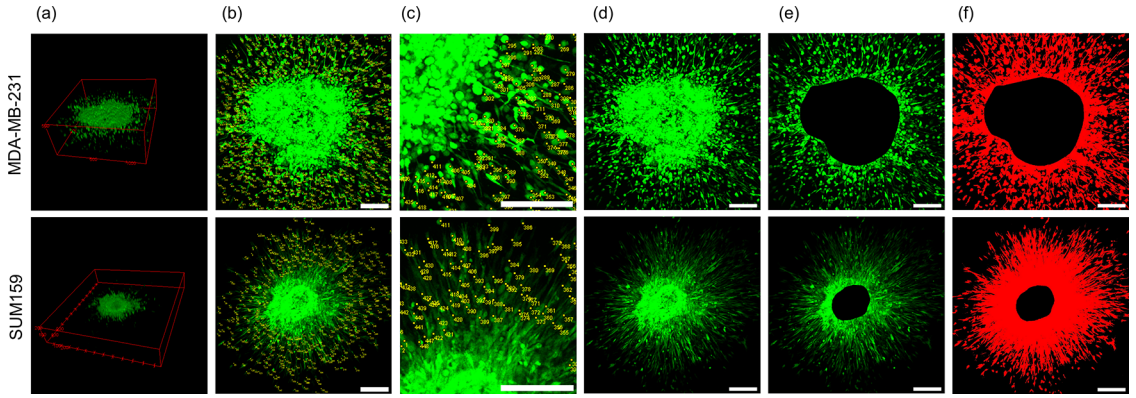

Figure 3. (a) 3D reconstructed view of spheroids of MDA-MB-231 cells and SUM159 cells. (b,c) 3D z-max-intensity-projection view of spheroid with points representing counts of invading cells. (d) 3D z-max-intensity-projection view of spheroids. (e) Spheroids after removing their cores. (f) Binary threshold of invading cells. Scale bars are 200 μm.

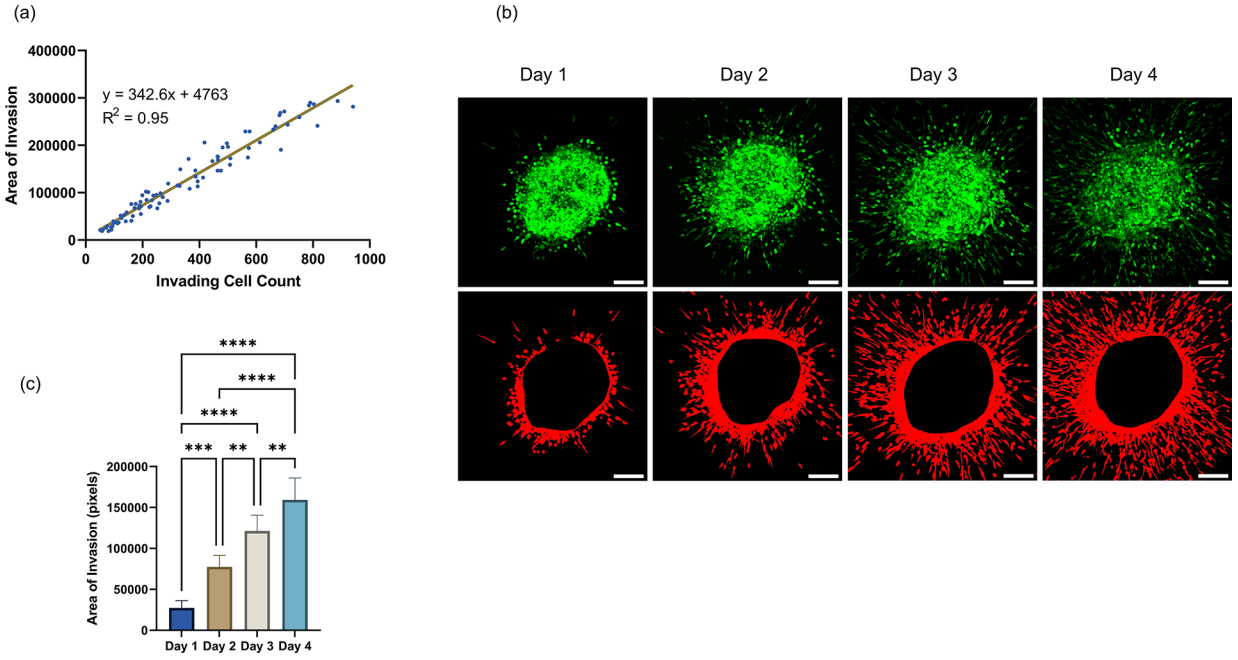

Figure 4. (a) Area of cell invasion from MDA-MB-231 spheroids is shown versus count of invading cells. (b,c) Area of invasion of MDA-MB-231 spheroids over 4 days and representative confocal images following maximum intensity z-projection and core removal and thresholding. Scale bars are 200 μm. $^{**}p < 0.01$, $^{***}p < 0.001$, $^{****}p < 0.0001$.

invasion that requires integrin-mediated cell adhesion to the ECM and its proteolytic degradation to generate paths for invasion, amoeboid-like invasion is achieved by deformation of cell nucleus and body and the development of bleblike protrusions of the membrane to enable the cell to squeeze through small pores within the ECM. Considering the significant difference in how these cells invade the 3D ECM, which is consistent with previous reports,[26,27] it is important to develop a method to conveniently and accurately quantify the different patterns of matrix invasion of cancer cells.

Quantifying Invading Cell Areas from Confocal Images

To quantify TNBC cell invasion from confocal microscope images, we adjusted the image from a 3D stack to a single 2D layer by using the maximum projection of the image stack (Figure 3a). First, we manually counted the number of cells invading from the core of spheroids into the collagen matrix (Figure 3b,c). This standard approach provides a direct measure of cell invasion and works well when cells, such as MDA-MB-231 cells, migrate individually. However, it is subject to errors when cells, such as SUM159 cells, invade collectively because it may count adjacent cells in each cluster as one object. In addition, the proximity of the invading clusters of cells makes it difficult to clearly segregate and quantify them as separate entities. To avoid this problem, we developed a simple method to measure the area of both invading single cells and clusters of cells. This method involved manually removing the core of the spheroid (Figure 3d,e) and applying thresholding based on pixel intensity to the resulting image to determine which pixels in the image belonged to invading cells (Figure 3f). This gave us the total pixel area of the invading cells, both individual cells and clusters.

Validating the Invading Cell Area Approach

We used two sets of studies to validate this method as a direct measure of cell invasion regardless of the mode of invasion. First, we evaluated the correlation between the invading cell area and the invading cell count from images of collagen-embedded tumor spheroids. This analysis used a representative sample of

https://doi.org/10.1021/acsmeasuresciau.3c00064
ACS Meas. Sci. Au 2024, 4, 260−266

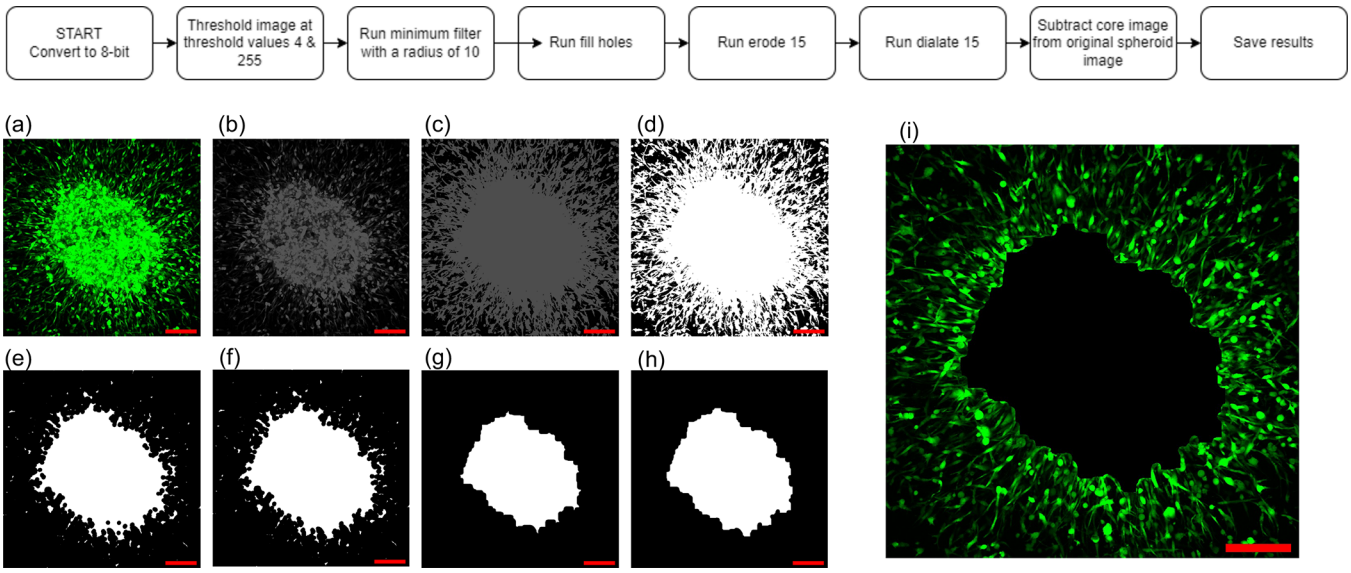

Figure 5. Process of automated core removal is shown for a spheroid of MDA-MB-231 cells. (a) Maximum intensity *z*-projection image, (b) initial image converted to an 8-bit image, (c,d) images after applying binary threshold, marking all pixels between values 4−255 inclusive, (e) image after applying minimum filter with a radius of 10, (f) image after applying fill holes filter, (g) image after applying erode filter for 15 iterations, (h) image after applying dilate filter for 15 iterations, and (i) final image after core is subtracted from the initial image. Scale bars are 200 μm.

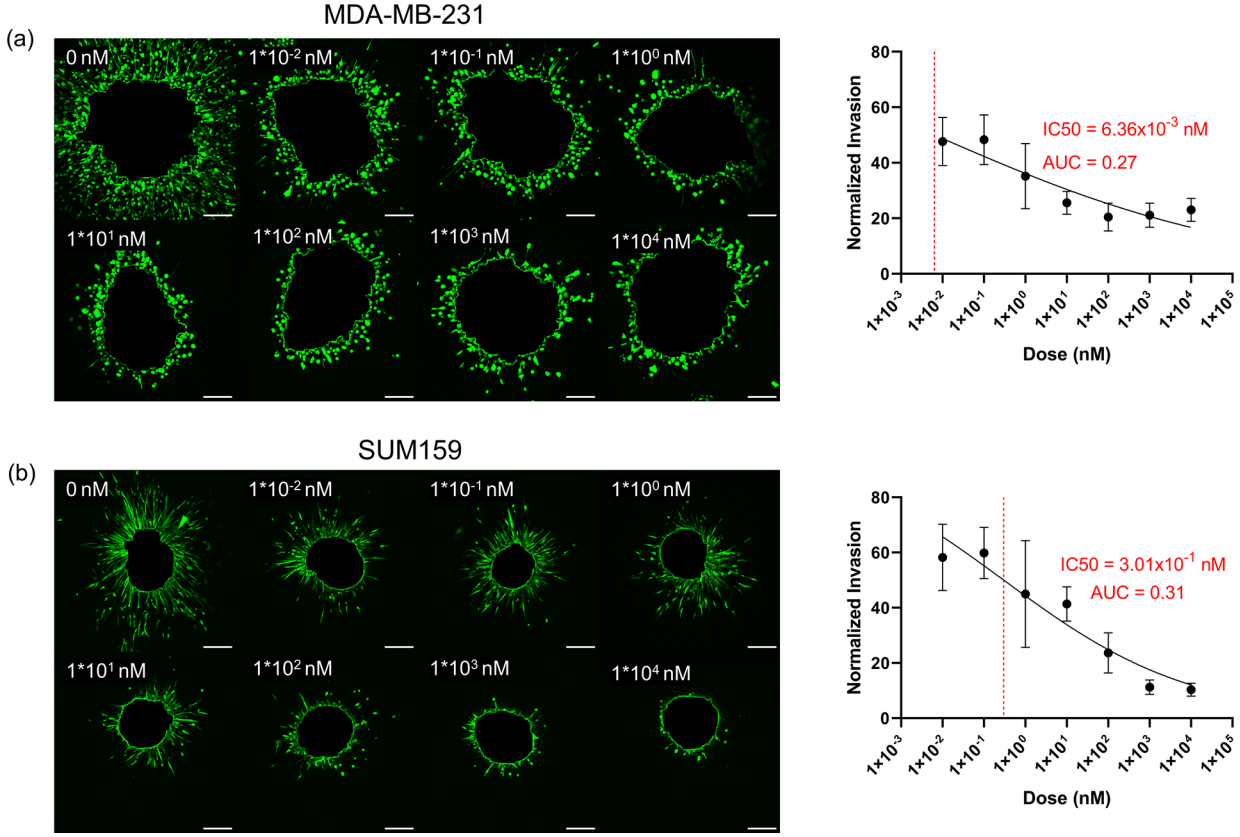

Figure 6. Paclitaxel treatment effect against matrix invasion of (a) MDA-MB-231 and (b) SUM159 tumor spheroids. Representative confocal images following core removal at different drug concentrations and respective dose−response curves are shown. Scale bars are 200 μm.

88 spheroids of MDA-MB-231 cells and led to a very strong linear correlation (R^2 = 0.95) (Figure 4a). Next, we computed the area of cell invasion from the same MDA-MB-231 spheroids over four different time points (Figure 4b). As expected, there were significant increases in the area of invasion over time (Figure 4c), consistent with the high motility of these cells reported previously.[28,29]

Automating the Process of Quantifying the Invading Cell Area

Due to the time-consuming and user-dependent process of manually removing the cores of spheroids for this analysis, we

https://doi.org/10.1021/acsmeasuresciau.3c00064
ACS Meas. Sci. Au 2024, 4, 260−266

developed an automated process to eliminate the inconsistency inherent to the manual process. Using FIJI, first, we converted the maximum projected image to an 8-bit image to allow for thresholding (Figure 5a,b). Next, we applied a threshold to mark all pixels with values between 4 and 255 inclusive, which roughly creates a binary mask of all the cells, i.e., objects of interest, in the image (Figure 5c,d). Applying a minimum filter with a radius of 10 removed the mask from most of the invading cells (Figure 5e). Then, we used the "fill holes" transform to add any holes in the core of the spheroid back to the mask followed by an erode filter with 15 iterations to remove any of the remaining bits of invading cells (Figure 5f,g). We applied a dilate filter to the mask for 15 iterations to grow the core mask back to its original size (Figure 5h). Finally, we subtracted the core mask from the original maximum projected image to generate an image of only the invading cells (Figure 5i). This automated process reduced the processing time of each individual image from minutes to seconds while consistently removing the core of spheroids prior to quantifying the invading cell area. We note that the minimum filter radius, the number of iterations during erosion and dilation steps, and the initial threshold value may need optimization adjustments depending on cell size, cell morphology, invasion mode, and microscope setting during imaging. However, across two cell lines that showed distinct invasion characteristics that are typically observed in cancer invasion assays, the selected values worked well.

Applying the Invading Cell Area Method to Drug Testing Studies

Next, we performed a proof-of-concept study to demonstrate the utility of this method in high throughput drug screening against cancer cells in 3D cultures. We treated the collagen-embedded MDA-MB-231 and SUM159 spheroids with paclitaxel dose-dependently in a concentration range of $0-10^4$ nM and used nontreated cultures as negative controls. Treatments lasted 4 days for MDA-MB-231 cells and 6 days for SUM159 cells due to the differences in the relative invasiveness of these two cell lines. After capturing confocal images of the cultures, we used the above-automated process to quantify the invading cell area. For each TNBC cell line, we normalized matrix invasion at different concentrations to the respective negative control and generated a dose−response graph (Figure 6). Paclitaxel had a 50% inhibitory concentration of 6.36×10^{-3} nM against MDA-MB-231 cells. The largest inhibitory effect happened with 10^2 nM paclitaxel, where the normalized invading cell area reduced to 20.4%. Increasing the drug concentration beyond 10^1 nM only marginally affected the matrix invasion of MDA-MB-231 cells. With SUM159 cultures, paclitaxel gave a 50% inhibitory concentration of 3.01×10^{-1} nM and showed the largest inhibitory effect at 10^3 nM. More increases in the drug concentration did not further reduce cell invasion. These results indicate that paclitaxel reduces the invasiveness of MDA-MB-231 cells at low nanomolar concentrations more effectively than matrix invasion of SUM159 cells. We also computed the normalized area under the curve (AUC) that shows the overall effect of a treatment. AUC ranges between 0 and 1, with 0 indicating a complete inhibition and 1 indicating no inhibition of invasion.[30] This analysis gave AUC values of 0.27 for MDA-MB-231 and 0.31 for SUM159 cells, indicating that over a wide concentration range, paclitaxel generated a relatively stronger inhibitory effect against MDA-MB-231 invasion.

CONCLUSIONS

We developed an automated method to quantify the matrix invasion of cancer cells from spheroid cultures. This technique reliably resolved matrix invasion for cancer cell lines with different invasion modalities as well as temporal changes in the extent of cell invasion and anti-invasive effects of a chemotherapy drug. Compared with existing methods, the high efficiency of this approach allows for significantly faster and more consistent analysis of cancer cell invasion to enable greater sample sizes and higher throughput of experiments such as screening of chemical compounds without a significant increase in costs or effort. This approach can also conveniently be adapted in various research laboratories studying 3D cancer cell invasion in more complex models of the tumor microenvironment and for mechanistic studies of therapeutic discoveries against cancer invasion.

ASSOCIATED CONTENT

Supporting Information

The Supporting Information is available free of charge at https://pubs.acs.org/doi/10.1021/acsmeasuresciau.3c00064.

"Remove Core" script prompts the user for an input folder containing .png image files of invading cells from spheroids and an output folder where the edited images will be stored. "Size and Circularity" script iterates through an input folder of .png files to measure the size and circularity of spheroids in each image (ZIP).

AUTHOR INFORMATION

Corresponding Author

Hossein Tavana − *Department of Biomedical Engineering, The University of Akron, Akron, Ohio 44325, United States;* orcid.org/0000-0003-3872-1869; Phone: (330) 972-6031; Email: tavana@uakron.edu

Author

Jacob Heiss − *Department of Biomedical Engineering, The University of Akron, Akron, Ohio 44325, United States*

Complete contact information is available at: https://pubs.acs.org/10.1021/acsmeasuresciau.3c00064

Author Contributions

CRediT: **Jacob Heiss** conceptualization, data curation, formal analysis, investigation, methodology, software, validation, visualization, writing-original draft, writing-review & editing; **Hossein Tavana** conceptualization, data curation, funding acquisition, investigation, methodology, project administration, resources, supervision, validation, writing-review & editing.

Notes

The authors declare no competing financial interest.

ACKNOWLEDGMENTS

This research was funded by grants CA225549 from NIH and 2140104 from NSF.

REFERENCES

(1) Lu, J.; et al. Breast Cancer Metastasis: Challenges and Opportunities. *Cancer Res.* **2009**, *69* (12), 4951−4953.
(2) Brabletz, S.; et al. Dynamic EMT: a multi-tool for tumor progression. *EMBO J.* **2021**, *40* (18), No. e108647.

(3) Scheel, C.; et al. Paracrine and autocrine signals induce and maintain mesenchymal and stem cell states in the breast. *Cell* **2011**, *145* (6), 926−940.
(4) Zhang, S.; et al. Inhibition of chemotherapy resistant breast cancer stem cells by a ROR1 specific antibody. *Proc. Natl. Acad. Sci. U. S. A.* **2019**, *116* (4), 1370−1377.
(5) Buschhaus, J. M.; et al. Targeting disseminated estrogen-receptor-positive breast cancer cells in bone marrow. *Oncogene* **2020**, *39* (34), 5649−5662.
(6) Singh, A.; Settleman, J. EMT, cancer stem cells and drug resistance: an emerging axis of evil in the war on cancer. *Oncogene* **2010**, *29* (34), 4741−4751.
(7) Graziani, V.; et al. The amoeboid state as part of the epithelial-to-mesenchymal transition programme. *Trends in Cell Biology* **2022**, *32* (3), 228−242.
(8) Wang, X.; et al. Collective invasion of cancer: Perspectives from pathology and development. *Pathology International* **2016**, *66* (4), 183−192.
(9) Raudenská, M.; et al. Engine shutdown: migrastatic strategies and prevention of metastases. *Trends in Cancer* **2023**, *9* (4), 293−308.
(10) Tavana, H.; et al. Polymeric Aqueous Biphasic System Rehydration Facilitates High Throughput Cell Exclusion Patterning For Cell Migration Studies. *Adv. Funct Mater.* **2011**, *21* (15), 2920−2926.
(11) Lemmo, S.; Nasrollahi, S.; Tavana, H. Aqueous biphasic cancer cell migration assay enables robust, high-throughput screening of anti-cancer compounds. *Biotechnol J.* **2014**, *9* (3), 426−434.
(12) Coughlin, M. F.; Kamm, R. D. The Use of Microfluidic Platforms to Probe the Mechanism of Cancer Cell Extravasation. *Adv. Healthcare Mater.* **2020**, *9* (8), No. 1901410.
(13) Shin, D. S.; Anseth, K. S. Recent advances in 3D models of tumor invasion. *Current Opinion in Biomedical Engineering* **2021**, *19*, No. 100310.
(14) Conti, S.et al.CAFs and Cancer Cells Co-Migration in 3D Spheroid Invasion Assay. In *The Epithelial-to Mesenchymal Transition: Methods and Protocols*; Campbell, K.; Theveneau, E., Eds.; Springer US: New York, NY, 2021; pp 243−256.
(15) Lee, S.; et al. Cancer-associated fibroblasts activated by miR-196a promote the migration and invasion of lung cancer cells. *Cancer Letters* **2021**, *508*, 92−103.
(16) Lamichhane, A.; et al. Therapeutic Targeting of Cancer Stem Cells Prevents Resistance of Colorectal Cancer Cells to MEK Inhibition. *ACS Pharmacology & Translational Science* **2022**, *5* (9), 724−734.
(17) Vinci, M.; Box, C.; Eccles, S. A. Three-dimensional (3D) tumor spheroid invasion assay. *J. Vis. Exp.* **2015**, *99*, No. e52686.
(18) Tavana, H.; et al. Nanolitre liquid patterning in aqueous environments for spatially defined reagent delivery to mammalian cells. *Nat. Mater.* **2009**, *8* (9), 736−741.
(19) Atefi, E.; et al. High Throughput, Polymeric Aqueous Two-Phase Printing of Tumor Spheroids. *Adv. Funct. Mater.* **2014**, *24* (41), 6509−6515.
(20) Thakuri, P. S.; et al. Quantitative Size-Based Analysis of Tumor Spheroids and Responses to Therapeutics. *Assay Drug Dev Technol.* **2019**, *17* (3), 140−149.
(21) Cristini, V.; et al. Morphologic instability and cancer invasion. *Clin. Cancer Res.* **2005**, *11* (19 Pt 1), 6772−6779.
(22) Chen, W.; et al. High-throughput image analysis of tumor spheroids: a user-friendly software application to measure the size of spheroids automatically and accurately. *J. Vis. Exp.* **2014**, *89*, 51639 DOI: 10.3791/51639.
(23) Piccinini, F. AnaSP: a software suite for automatic image analysis of multicellular spheroids. *Comput. Methods Programs Biomed* **2015**, *119* (1), 43−52.
(24) Lehmann, B. D.; et al. Identification of human triple-negative breast cancer subtypes and preclinical models for selection of targeted therapies. *J. Clin. Invest.* **2011**, *121* (7), 2750−2767.
(25) Grigoriadis, A.; et al. Molecular characterisation of cell line models for triple-negative breast cancers. *BMC Genomics* **2012**, *13* (1), 619.
(26) Liu, C.; et al. Hybrid collagen alginate hydrogel as a platform for 3D tumor spheroid invasion. *Acta Biomater* **2018**, *75*, 213−225.
(27) Fatherree, J. P.; et al. Chemotherapy-Induced Collagen IV Drives Cancer Cell Motility through Activation of Src and Focal Adhesion Kinase. *Cancer Res.* **2022**, *82* (10), 2031−2044.
(28) Singh, S.; et al. Organotypic breast tumor model elucidates dynamic remodeling of tumor microenvironment. *Biomaterials* **2020**, *238*, No. 119853.
(29) Singh, S.; et al. Therapeutic Targeting of Stromal-Tumor HGF-MET Signaling in an Organotypic Triple-Negative Breast Tumor Model. *Molecular Cancer Research* **2022**, *20* (7), 1166−1177.
(30) Shahi Thakuri, P.; et al. Multiparametric Analysis of Oncology Drug Screening with Aqueous Two-Phase Tumor Spheroids. *Mol. Pharmaceutics* **2016**, *13* (11), 3724−3735.

https://doi.org/10.1021/acsmeasuresciau.3c00064
ACS Meas. Sci. Au 2024, 4, 260−266